ACS Catalysis

pubs.acs.org/acscatalysis

Research Article

Understanding the Role of Electronic Effects in CO on the Pt−Sn Alloy Surface via Band Structure Measurements

Jongkeun Jung, Sungwoo Kang, Laurent Nicolaï, Jisook Hong, Ján Minár, Inkyung Song, Wonshik Kyung, Soohyun Cho, Beomseo Kim, Jonathan D. Denlinger, Francisco José Cadete Santos Aires, Eric Ehret, Philip Ross, Jihoon Shim, Slavomir Nemšák, Doyoung Noh, Seungwu Han,* Changyoung Kim,* and Bongjin Simon Mun*

Cite This: *ACS Catal.* 2022, 12, 219−225

Read Online

ACCESS | Metrics & More | Article Recommendations | Supporting Information

ABSTRACT: Using angle-resolved photoemission spectroscopy, we show direct evidence for charge transfer between adsorbed molecules and metal substrates, i.e., chemisorption of CO on Pt(111) and Pt−Sn/Pt(111) 2 × 2 surfaces. The observed band structures show a unique signature of charge transfer as CO atoms are adsorbed, revealing the roles of specific orbital characters participating in the chemisorption process. As the coverage of CO increases, the degree of charge transfer between CO and Pt shows a clear difference to that of Pt−Sn. With comparison to density functional theory calculation results, the observed distinct features in the band structure are interpreted as back-donation bonding states formed between the Pt molecular orbital and the 2π orbital of CO. Furthermore, the change in the surface charge concentration, measured from the Fermi surface area, shows that the Pt surface has a larger charge concentration change than the Pt−Sn surface upon CO adsorption. The differences between Pt and Pt−Sn surfaces are due to the effect of Pt−Sn intermetallic bonding on the interaction of CO with the surface.

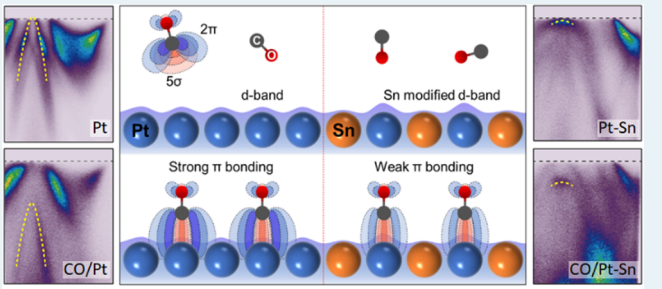

Energy shift band of Pt and Pt-Sn surface alloy due to CO adsorption

KEYWORDS: *angle-resolved photoelectron spectroscopy, CO adsorption, Pt alloy, π back-donation, orbital character*

INTRODUCTION

In heterogeneous catalysis, knowledge of surface electronic structures provides critical insight for understanding fundamental surface chemical reactivity of a material.[1,2] Conversely, the desired chemical properties could be realized via modifying electronic structures of materials. In surface catalysis, the latter approach has been the major driving force for finding ideal surface catalysts. In this regard, the frontier molecular orbital model has been intensively studied to explain the basic surface chemical reaction route.[3]

Later, based on the information on the *d*-band structure and chemical properties, Nørskov *et al.* suggested that the anticipated surface chemical properties could be obtained by tuning the electronic structures of alloys with optimum elements.[4,5] In this so-called *d*-band model, the structure of the *d*-band near the E_F (Fermi level) displays strong correlation with the surface chemical reaction. Often, the *d*-band model is readily used in selecting the effective alloying components to maximize the synergistic effects between participating alloy elements in heterogeneous catalysts.[6,7]

As a representative study of bimetallic alloy catalysts, the Pt−Sn alloy has been thoroughly studied. Using XPS and DFT calculation, Rodriguez *et al.* pointed out that the presence of charge transfer from Sn to Pt as well as subsequent rehybridization between Pt−Sn generates unique surface chemistry of SO_2, suggesting that both ensemble and electronic effects are important in the reaction.[8] In an STM study, Koel *et al.* explored the sign of charge modulation near the E_F of a Pt−Sn alloy surface, e.g., the reduction of electron density near the E_F at the Pt site, and interpreted the electronic structure modulation as a measure of chemical reactivity.[9] On the theoretical side, Sautet and Delbecq calculated the amount of charge transfer from Sn to Pt depending on the surface structure of Sn.[10] It was pointed out in the work that the *d*-band center is shifted downward due to the charge rearrangement, highlighting the role of the electronic structure due to the amount of neighboring Sn atoms.

While the major aspect of the electronic structure change has been discussed on Pt−Sn systems, there is no decisive

Received: October 4, 2021
Revised: November 29, 2021
Published: December 14, 2021

experimental evidence for the modified Pt electronic structure due to Sn alloying and its participation on surface chemical reactions. Detailed information on the orbital-dependent electronic structure of Pt−Sn and charge transfer in the chemical reaction can provide significant insight into the nature of reactivity of Pt−Sn alloys. It in turn can be beneficial for the development of advanced alloy catalysts. Nonetheless, information on such an orbital-dependent electronic structure and its effect on the catalytic reaction has not been obtained due to the lack of a suitable tool to investigate the issue.

We resolve the issue by studying ordered CO molecules on Pt(111) and Pt−Sn(111) surface alloys using angle-resolved photoemission spectroscopy (ARPES) and DFT calculations. CO adsorption on an ordered surface enables us to monitor the band dispersion change due to the interaction between CO molecular orbitals and surface electronic structures of Pt−Sn alloys. In comparison with DFT calculations, the enhanced spectral features near the E_F are identified as d_{xz} and d_{yz} orbitals of the π bonding. The charge transfer mechanism deduced from the band structure near the E_F is found to be described by a combination of the π and σ bonding interactions in the Blyholder model.[11] Inspection of the band structure during a chemical reaction reveals the key role of electronic effects in a Pt−Sn alloy. This method can be applied to studies of other metal-based catalyst systems.

EXPERIMENTAL AND COMPUTATIONAL METHODS

Experimental Methods. Clean Pt(111) surfaces were prepared by repeating Ar sputtering and annealing at 1000 K. A Pt−Sn/Pt(111) 2 × 2 surface alloy was fabricated by Sn deposition and annealing on a Pt(111) single crystal surface at 1100 K. The surface arrangements of Pt(111), Pt−Sn/Pt(111) surface alloy, and CO-adsorbed samples were monitored by LEED (Figure S2). ARPES measurements were performed in a laboratory-based system, equipped with a Scienta DA30 analyzer. The energy resolution was 8 meV at a 21.2 eV photon energy, and the angular resolution was 0.1°, which corresponds to a momentum resolution of 0.002 Å^{-1}. CO molecules were dosed at 100 K for both Pt and Pt−Sn/Pt(111) surfaces. ARPES and LEED were performed at 10 K for pristine and 100 K for CO-adsorbed samples. All measurements were performed in an ultrahigh vacuum chamber with a base pressure less than 4 × 10^{-11} Torr. More experimental details can be found in the Supporting Information.

Computational Details. The DFT calculations were performed with the Vienna ab initio simulation package (VASP).[12] The revPBE-vdW-DF exchange−correlation functional was used to describe the electron−electron interaction.[13] This functional is known to correctly describe the order of adsorption energies of CO on Pt sites.[14] We also checked that the use of the PBE functional with the Hubbard U correction,[15,16] which could resolve the Pt puzzle,[17] led to similar results. A Pt slab with twelve layers was used with an ∼10 Å vacuum region. To calculate the Pt/Sn structure, atomic structures were relaxed until the atomic force acting on each atom was reduced under 0.03 eV/Å. For the bare Pt slab, the structure geometry was fully optimized. On the other hand, for the structures of supercells (CO-adsorbed structures and Sn-doped structures), only the top four layers were allowed to move, while the bottom eight layers were fixed. A 10 × 10 × 1 k-point mesh for Brillouin zone (BZ) sampling was used as a unit cell, and for supercells, the number of mesh was reduced in proportion to the surface area. Band unfolding was performed using the BandUP code.[18,19] The atomic models used for DFT calculations are shown in Figure S3.

RESULTS AND DISCUSSION

Figure 1a shows the structures of Pt(111) and Pt−Sn/Pt(111) 2 × 2 surfaces. The 1 × 1 and 2 × 2 unit cells for Pt and the Pt−Sn/Pt(111) surface alloy, respectively, are indicated by black dashed lines. In the Pt−Sn/Pt(111) 2 × 2 surface alloy, Sn atoms (shown in red) replace surface Pt atoms to form a 2

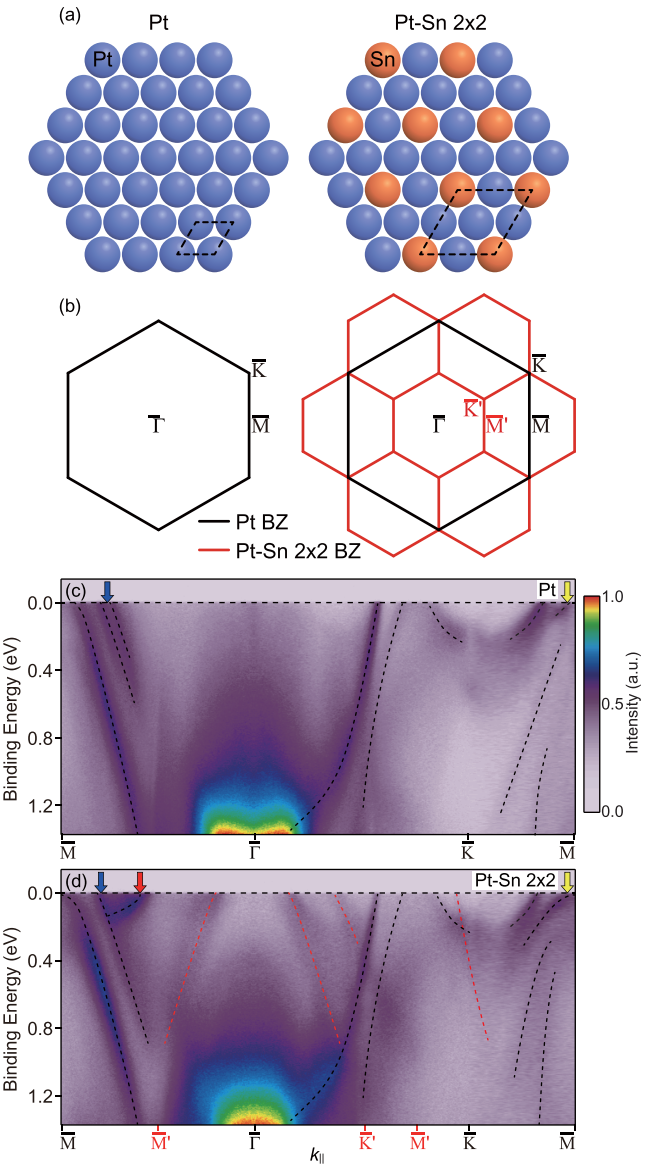

Figure 1. ARPES measurements of the k-space-resolved electronic structure. (a) Top view showing the Pt(111) and Pt−Sn/Pt(111) 2 × 2 crystal structures. Black dashed lines represent the 1 × 1 and 2 × 2 unit cells. (b) Brillouin zone of Pt (black hexagon) and 2 × 2 folded Brillouin zone of the Pt−Sn/Pt(111) 2 × 2 surface alloy (red hexagons). The electronic structures of (c) Pt(111) surface and (d) Pt−Sn/Pt(111) 2 × 2 surface alloy shown with guidelines. The red dotted lines represent Pt−Sn/Pt(111) 2 × 2 folded bands; unfolded bands are indicated by black dotted lines. The differences in the band structure between Pt and the unfolded Pt−Sn/Pt(111) 2 × 2 surface alloy are marked with blue, red, and yellow arrows.

https://doi.org/10.1021/acscatal.1c04566
ACS Catal. 2022, 12, 219−225

× 2 unit cell. The surface BZ is reduced for Pt−Sn/Pt(111) due to the larger 2 × 2 surface unit cell (Figure 1b). The bands outside the 2 × 2 BZ are folded about the BZ boundary to form a new band structure, a phenomenon called band folding.

We first use ARPES data to identify the band structures of clean Pt(111) and Pt−Sn/Pt(111) 2 × 2 surfaces, as shown in Figure 1b,c. These high-symmetry cut data show various dispersive bands with identified bands marked with black dotted lines. As mentioned above, band folding takes place due to the 2 × 2 surface reconstruction of the Pt−Sn/Pt(111) surface. This explains the greater number of bands observed for the Pt−Sn/Pt(111) surface in Figure 1d compared to the Pt(111) surface in Figure 1c. To distinguish the original and folded bands, guidelines are superimposed onto the Pt−Sn/Pt(111) ARPES data in Figure 1d. Black dotted lines indicate the original band structure, while red dotted lines indicate folded bands. It is important to note that the folded bands at the Γ point originate from unfolded bands at the M point. This band folding effect is even more evident in the Fermi surface map data and will be discussed later.

While the unfolded band structure of Pt−Sn/Pt(111) along the Γ−K direction in Figure 1d is similar to that of Pt in Figure 1c, significant differences exist between these two sets of data, indicated by blue, yellow, and red arrows. While apparent band splitting can be seen on the Pt surface near the M point, no such feature is discernable on the Pt−Sn/Pt(111) 2 × 2 surface (blue arrow). The band indicated by the red arrow is a new band that is not observed at the Pt surface. In addition, the shape of the band on the M−K line near the E_F (marked by the yellow arrow) differs between the two surfaces. These differences in the band structure are due to the surface alloying of Pt and Sn.

Next, we investigate the effect of CO adsorption on the electronic structure of the metal surfaces. To better understand the correlation between the band structure and adsorption, the transient surface electronic structures are monitored as CO is adsorbed onto the surfaces of Pt(111) and 2 × 2 Pt−Sn/Pt(111). Figure 2 shows the Fermi surface evolution of these surfaces upon CO dosing. Distinct differences in the Fermi surface at the Γ and M points are observed when comparing clean Pt(111) (Figure 2a) and Pt−Sn/Pt(111) 2 × 2 (Figure 2d). The pocket at Γ on the Pt−Sn/Pt(111) surface is due to folded bands from the M point, i.e., the folded bands at Γ in Figure 1d, and thus looks similar to the pocket near the M point. These folded bands around Γ confirm the presence of the 2 × 2 superstructure of the Pt−Sn/Pt(111) surface. On the other hand, the hole pocket (Fermi surface of a hole band) at the M point, which is also seen in Figure 1, is larger for the Pt−Sn/Pt(111) 2 × 2 surface compared to Pt. By comparing the experimental dispersion with Korringa−Kohn−Rostoker calculation results,[20] we find that the enlargement of the hole pocket at the M point is due to the hybridization between Sn and Pt. The ARPES simulation data (Figure S4a,b in the Supporting Information) show details of the Fermi surface topology and match the experimental results shown in Figure 2a,d. The presence of band folding is also reproduced in the calculation results and accounts for the multiple Fermi surfaces of the Pt−Sn/Pt(111) 2 × 2 surface.

The data in Figure 2 show that significant changes occur in the electronic structures of the Pt and Pt−Sn/Pt(111) surfaces as CO molecules are adsorbed. One particularly notable change upon CO adsorption is the splitting of the large hexagonal Fermi surface of Pt, centered at Γ. This Fermi

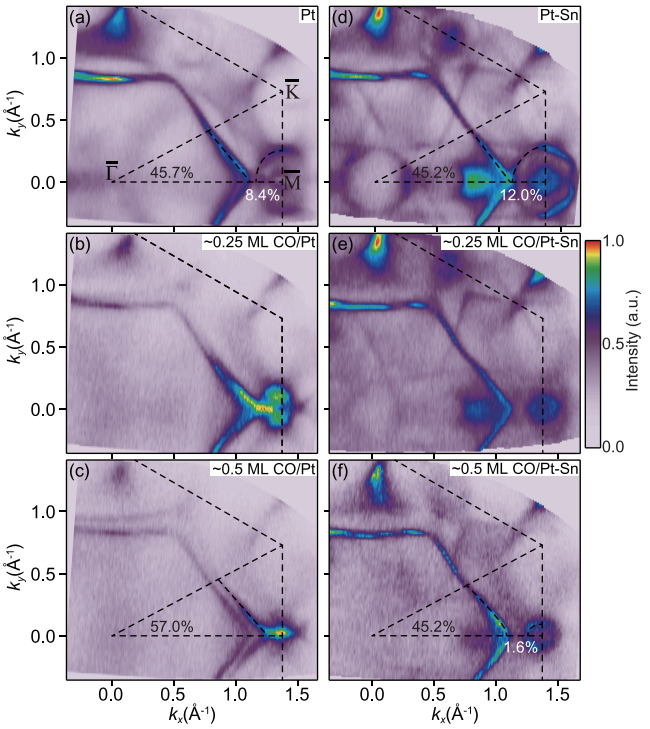

Figure 2. Pristine Fermi surfaces of Pt(111) and the Pt−Sn/Pt(111) 2 × 2 surface alloy shown along with changes in the Fermi surfaces caused by CO adsorption. Fermi surface maps shown for (a) Pt(111), (b) ~0.25 ML CO/Pt(111), (c) ~0.5 ML CO/Pt(111), (d) Pt−Sn/Pt(111) surface alloy, (e) ~0.25 ML CO/Pt−Sn/Pt(111) surface alloy, and (f) ~0.5 ML CO/Pt−Sn/Pt(111) surface alloy. Dashed lines indicate the BZ boundary.

surface splitting is attributed to the differential responses of surface and bulk bands of Pt to the adsorption of CO, resulting in the formation of bulk and surface states. With comparison to DFT, the splitting bands are mostly composed of in-plane orbitals, an explicit sign of surface bands (Figures S5 and S6). Interestingly, this splitting is not observed with Pt−Sn/Pt(111), indicating the modification of the surface band of Pt upon Sn alloying, which leads to an entirely different response to CO adsorption.

More importantly, the Fermi surface pocket of Pt(111) centered at M becomes smaller as CO is adsorbed. The data in Figure 2a−c show that the pocket at the M point of Pt almost disappears with adsorption of the ~0.5 monolayer (ML) of CO. This reduction in the pocket size is less dramatic for Pt−Sn/Pt, as shown in Figure 2d−f, with a finite Fermi pocket remaining at ~0.5 ML coverage. Since changes to the hole bands at M occur on both the Pt and Pt−Sn/Pt surfaces with CO adsorption, we examine the associated changes in the electronic structure near the Fermi surfaces of both systems more closely.

First, we calculate the charge concentrations of each system. Previously, based on DFT calculations and within the Blyholder model, Kalhara Gunasooriya and Saeys found that the charge redistribution at Pt sites due to π and σ bonding affects the CO adsorption behavior as the coverage of CO increases.[21] In our ARPES study, the change in the surface charge carrier was monitored using the Luttinger theorem. According to the Luttinger theorem, the area enclosed by the Fermi surface is proportional to the carrier number.[22,23] Thus, the number of conduction electrons of a system changed by

https://doi.org/10.1021/acscatal.1c04566
ACS Catal. 2022, 12, 219−225

CO adsorption can be obtained from the change in the electron and hole pocket sizes on the Fermi surface (Figure 2) For Pt, the proportion of the large hexagonal pocket in the BZ is 45.7%, and that of the M point hole pocket is 8.4%. At ∼0.5 ML CO/Pt(111), the M point hole pocket vanishes, and the surface hexagon pocket becomes 57% of the BZ. These changes indicate an increase in electron charge concentration of 0.394 electrons per unit cell ((57 − 45.7 + 8.4) × 2 = 39.4 (%)). For Pt−Sn/Pt(111), the size of the hexagonal band before and after CO adsorption remained unchanged with a reduction in the size of the hole band from 12.0 to 1.6%. This indicates an increase of 0.208 electrons per 1 × 1 Pt unit cell due to CO adsorption ((12.0 − 1.6) × 2 = 20.8 (%)). The change in the number of conduction electrons due to CO adsorption on Pt(111) is almost twice that of the Pt−Sn/Pt(111) surface alloy.

Next, we closely examined the band dispersion near M, which shows a significant change in the Fermi surface topology upon CO dosing. Figure 3 shows the measured electronic

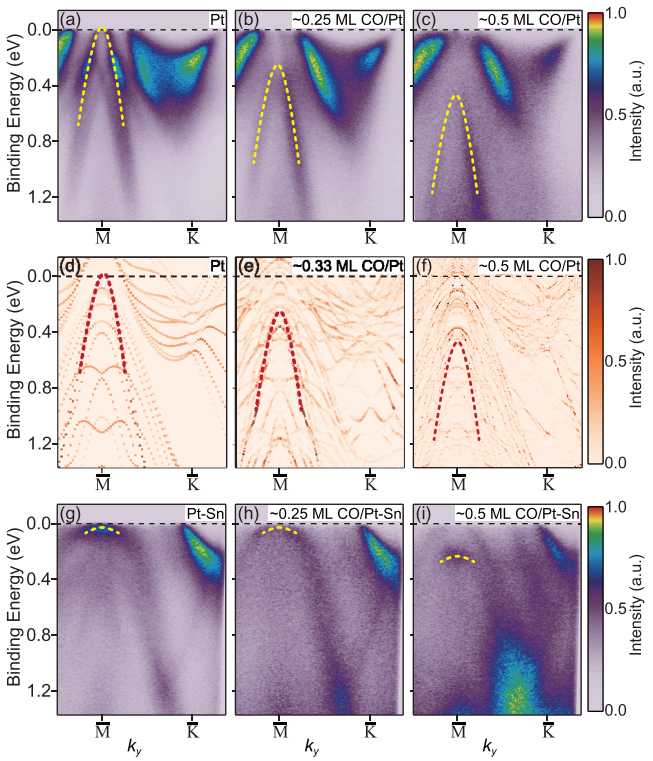

Figure 3. CO-induced band shifts for Pt and the Pt−Sn/Pt(111) surface alloy. Band structures of (a) Pt(111), (b) ∼0.25 ML CO/Pt(111), (c) ∼0.5 ML CO/Pt(111), (g) Pt−Sn/Pt(111) surface alloy, (h) ∼0.25 ML CO/Pt−Sn/Pt(111) surface alloy, and (i) ∼0.5 ML CO/Pt−Sn/Pt(111) surface alloy shown at the M point. Yellow dotted lines are provided as the guide to the eyes for significant shifts induced by the CO adsorbate. Theoretical (d) Pt(111), (e) ∼0.33 ML CO/Pt(111), and (f) ∼0.5 ML CO/Pt(111) band structures shown for comparison. Red dotted lines are duplicated from yellow dotted lines in (a−c).

structures of Pt(111) and Pt−Sn/Pt(111) 2 × 2 along the M−K high-symmetry cut for CO coverages of 0, 0.25, and 0.5 ML. To identify the molecular orbitals participating in the charge exchange between CO and Pt, the results of DFT calculations are shown in Figure 3d−f. In DFT calculation results, the contribution from only the top surface layer is shown, and the red dotted lines are drawn to help the comparison with the experimental results. In addition, the simulated electronic structures of pristine Pt(111) and Pt−Sn/Pt(111) surfaces are shown in Figure S4c,d.

In comparing the band features near M in Figure 3a,g, we note that the bands of Pt−Sn/Pt(111) are generally broader than those of Pt. The broader bands of the Pt−Sn/Pt(111) alloy, which are consistent with theoretical results (Figure S4c,d), arise from hybridization with Sn and further indicate the modification of the electronic structure. Adsorption of CO results in a downward shift of the hole bands at the M point for both Pt and Pt−Sn/Pt(111) surfaces, as indicated by the yellow dotted lines. Note that this shift occurs only for the hole bands at the M point, indicating that only certain bands participate in bonding during adsorption. The band shows a rigid shift, with little or no broadening. This downshifted band is also identified in the DFT results in Figure 3d−f. We found that the orbital character of the band shows an increased contribution from out-of-plane orbitals, as listed in Table 1.

Table 1. Orbital Character Change of the Energy Shifting Band and the Calculated Orbital Contribution for the Energy Shifting Band of Pt during CO Adsorption on Figure 3a−c[a]

material	binding energy [eV]	d_{z^2} contribution	$d_{xz} + d_{yz}$ contribution	$d_{xy} + d_{x^2-y^2}$ contribution
Pt	0.08	0.592	0.180	0.107
0.33 ML CO/Pt	0.35	0.388	0.276	0.076
0.5 ML CO/Pt	0.48	0.297	0.420	0.038

[a]Binding energy represents the position of the energy shifting band at the M point.

This finding clearly supports the π bonding characteristics of the back-donation, which occurs near the E_F, i.e., d_{xz} and d_{yz} components from Pt to CO in the picture of the Blyholder model.[11]

While the downward shift of hole bands is similar between Pt and Pt−Sn/Pt(111), a close examination of the band behavior reveals several distinct differences. While the hole band of Pt shifts downward continuously with CO coverage, that of Pt−Sn/Pt(111) does not shift until the CO coverage reaches ∼0.5 ML. This suggests that CO molecules on Pt−Sn/Pt(111) form an ordered surface only above a certain coverage as only the ordered structure is expected to contribute to the dispersive bands. This observation agrees with the result of a previous report,[24] wherein the LEED pattern of a Pt−Sn/Pt(111) surface does not change with CO coverage below a certain level. In addition, the Pt hole band shift for 0.5 ML CO is about 500 meV (yellow line in Figure 3c), while that for Pt−Sn/Pt(111) is only 200 meV (Figure 3i); that is, at 0.5 ML of CO, the hole band shift of the Pt surface is 2.5 times larger than that of the Pt−Sn/Pt(111) surface alloy, which again reflects the difference in the chemical bonding state between the two surfaces. In fact, DFT calculations show that the adsorption energy of CO on Pt(111) is larger than that of CO on the Pt−Sn alloy surface by 0.45 eV on average (see Table S1). This value is comparable to that of Dupont *et al.*, which varies from 0.16 to 0.33 eV depending on the CO coverage, adsorption site, and calculation method.[25]

Here, we wish to discuss the implication of our observations. The most significant change due to the Sn alloying is observed

https://doi.org/10.1021/acscatal.1c04566
ACS Catal. 2022, 12, 219−225

at the M point in Figure 3. The M point band shows a significant energy shift upon CO adsorption on both Pt and the Pt−Sn surface alloy. Considering the dominant contribution of *d*-band orbitals to the near E_F electronic structure (Figure S5) and the increasing contribution from out-of-plane orbitals to the downward shifting hole band at M, shown in Figure 3, the observed band downshift is a clear indicator of a π bonding between d orbitals of the metal and the 2π orbitals of CO during chemisorption of CO on the metal surface. Furthermore, the different amount of the downshift of the hole band between Pt and Pt−Sn surfaces clearly shows that the degree of participating back-donation charge is different, i.e., weaker bonding of the Pt−Sn surface, as schematically shown in Figure 4. In fact, this is indicated in the different changes in

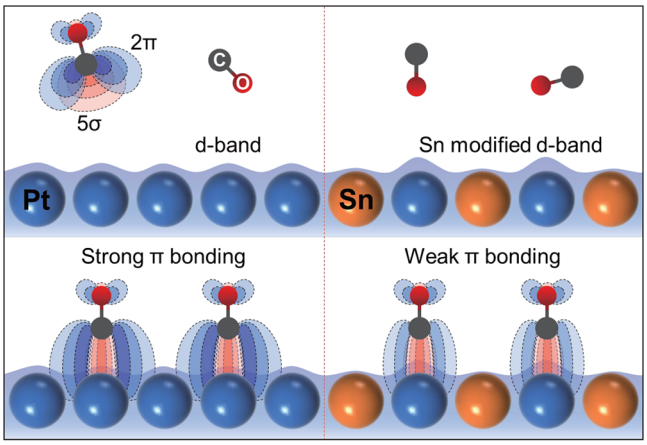

Figure 4. Schematic illustration of the role of Sn on the CO adsorption mechanism in Pt and the Pt−Sn alloy.

the number of conduction electrons calculated based on the Luttinger theorem in Figure 2. It is also to note that the increase in the conduction electron does not necessarily mean charge transfer from CO to Pt since what we observe in ARPES on the CO-adsorbed Pt surface are hybridized states between CO and Pt orbitals. In published DFT calculations, σ bonding states are identified at high binding energies (5−9 eV), while π back-donation states exist near the Fermi level.[26−28] Considering the energy positions of the states, the modification of the band structure that we observed at near the Fermi surface should mostly originate from π bonding states, which consist of Pt *d*-band and CO 2π states. The lesser change in the number of conduction electrons in Pt−Sn than Pt near the Fermi surface indicates a weaker charge interaction in the case of the Pt−Sn surface, consistent with the above picture of the smaller back-donation of *d*-bands in Pt−Sn. In addition, a theoretical study of CO on Pt clusters predicted that the downward shift of Pt *d*-bands participating in the back-donation is a few hundred meV, which is consistent with our experimental observations.[28] Overall, these observations indicate that Sn plays an important role in the determination of CO adsorption properties by modifying the electronic structure of Pt.

CONCLUSIONS

In summary, high-resolution ARPES measurements are used to directly observe transient bonding states of CO molecules on Pt and Pt−Sn/Pt(111) alloy surfaces. Energy shifts of hole bands and changes in the Fermi pocket size near the M point of both Pt and Pt−Sn/Pt(111) show the band structure with specific orbital characters participating in the bonding process. The observed electronic band structure change indicates the role of Sn as a modifier of the Pt electronic band structure. Moreover, the amount of charge transferred from adsorbed CO is measured from the Fermi surface pockets sizes, which can be related to the different CO bonding strength between Pt and the Pt−Sn surface alloy. Our ARPES results reveal the mechanism on how Sn affects the CO adsorption process on Pt and show the important role of the surface electronic structure in molecular adsorption reactions. Our results show how the *d*-bands with specific orbital characters participate in chemical bonding with CO molecules on surfaces, which is highly valuable information for understanding catalytic reactions at the molecular level. Furthermore, our methodology, i.e., ARPES on surface reactivity of Pt−Sn surface alloys, can be systematically expanded to other Pt-based bimetallic alloys, which can then unveil the nature of modified catalytic activity of alloy catalysts.

ASSOCIATED CONTENT

Supporting Information

The Supporting Information is available free of charge at https://pubs.acs.org/doi/10.1021/acscatal.1c04566.

Experimental details; (Figures S1−S7) AES data, LEED patterns, atomic models for DFT calculations, ARPES simulation for Pt and the Pt−Sn/Pt(111) 2×2 surface alloy, orbital character calculations, band structures, and second derivatives of CO-induced energy band shifts; (Tables S1 and S2) calculated average adsorption energies of CO and calculated orbital character change of the hexagonal band (PDF)

AUTHOR INFORMATION

Corresponding Authors

Seungwu Han − *Department of Materials Science and Engineering, Seoul National University, Seoul 08826, Republic of Korea;* orcid.org/0000-0003-3958-0922; Email: hansw@snu.ac.kr

Changyoung Kim − *Center for Correlated Electron Systems, Institute for Basic Science, Seoul 08826, Republic of Korea; Department of Physics and Astronomy, Seoul National University, Seoul 08826, Republic of Korea;* Email: changyoung@snu.ac.kr

Bongjin Simon Mun − *Department of Physics and Photon Science and Center for Advanced X-ray Science, Gwangju Institute of Science and Technology, Gwangju 61005, Republic of Korea;* orcid.org/0000-0002-8525-3298; Email: bsmun@gist.ac.kr

Authors

Jongkeun Jung − *Center for Correlated Electron Systems, Institute for Basic Science, Seoul 08826, Republic of Korea; Department of Physics and Astronomy, Seoul National University, Seoul 08826, Republic of Korea*

Sungwoo Kang − *Department of Materials Science and Engineering, Seoul National University, Seoul 08826, Republic of Korea;* orcid.org/0000-0001-8177-8815

Laurent Nicolaï − *New Technologies Research Centre (NTC), University of West Bohemia, Plzen 301 00, Czech Republic*

https://doi.org/10.1021/acscatal.1c04566
ACS Catal. 2022, 12, 219−225

Jisook Hong − *The Molecular Foundry, Lawrence Berkeley National Laboratory, Berkeley, California 94720, United States;* orcid.org/0000-0001-8331-3878
Ján Minár − *New Technologies Research Centre (NTC), University of West Bohemia, Plzen 301 00, Czech Republic*
Inkyung Song − *Center for Correlated Electron Systems, Institute for Basic Science, Seoul 08826, Republic of Korea; Department of Physics and Astronomy, Seoul National University, Seoul 08826, Republic of Korea*
Wonshik Kyung − *Center for Correlated Electron Systems, Institute for Basic Science, Seoul 08826, Republic of Korea; Department of Physics and Astronomy, Seoul National University, Seoul 08826, Republic of Korea;* orcid.org/0000-0001-8750-5471
Soohyun Cho − *Shanghai Institute of Microsystem and Information Technology (SIMIT), Chinese Academy of Sciences, Shanghai 200050, People's Republic of China;* orcid.org/0000-0002-2399-7179
Beomseo Kim − *Center for Correlated Electron Systems, Institute for Basic Science, Seoul 08826, Republic of Korea; Department of Physics and Astronomy, Seoul National University, Seoul 08826, Republic of Korea;* orcid.org/0000-0002-5210-6419
Jonathan D. Denlinger − *Advanced Light Source, Lawrence Berkeley National Laboratory, Berkeley, California 94720, United States*
Francisco José Cadete Santos Aires − *Université Claude Bernard Lyon 1, Université de Lyon, CNRS - UMR 5256, IRCELYON, 69626 Villeurbanne Cedex, France; National Research Tomsk State University, Laboratory for Catalytic Research, 634050 Tomsk, Russian Federation*
Eric Ehret − *Université Claude Bernard Lyon 1, Université de Lyon, CNRS - UMR 5256, IRCELYON, 69626 Villeurbanne Cedex, France*
Philip Ross − *Materials Science Division, Lawrence Berkeley National Laboratory, Berkeley, California 94720, United States*
Jihoon Shim − *Department of Chemistry, Pohang University of Science and Technology, Pohang 37673, Republic of Korea;* orcid.org/0000-0001-7357-0029
Slavomir Nemšák − *Advanced Light Source, Lawrence Berkeley National Laboratory, Berkeley, California 94720, United States;* orcid.org/0000-0002-6103-2925
Doyoung Noh − *Department of Physics and Photon Science and Center for Advanced X-ray Science, Gwangju Institute of Science and Technology, Gwangju 61005, Republic of Korea*

Complete contact information is available at: https://pubs.acs.org/10.1021/acscatal.1c04566

Author Contributions

The manuscript was written through contributions of all authors.

Notes

The authors declare no competing financial interest.

■ ACKNOWLEDGMENTS

The authors thank Byungmin Sohn for helping us draw a figure in the cover letter. This work was supported by the research program of the Institute for Basic Science (Grant No. IBS-R009-G2). Financial support was also provided by the National Research Foundation of Korea (NRF-2015R1A5A1009962, NRF-2017K1A3A7A09016316, NRF-2019R1A2C2008052, and NRF-2020K1A3A7A09080400), the GIST Research Institute Grant funded by the Gwangju Institute of Science and Technology (GIST) 2021, and the KISTI National Supercomputing Center (KSC-2020-CRE-0064). The Advanced Light Source is supported by the Office of Basic Energy Sciences of the U.S. DOE under Contract No. DE-AC02-05CH11231. This work was further supported by the European Regional Development Fund (ERDF), project CEDAMNF, reg. no. CZ.02.1.01/0.0/0.0/15_003/0000358.

■ REFERENCES

(1) Harrison, W. A. *Electronic Structure and the Properties of Solids: the Physics of the Chemical Bond*; Courier Corporation: 2012.
(2) Greeley, J.; Nørskov, J. K.; Mavrikakis, M. Electronic Structure and Catalysis on Metal Surfaces. *Annu. Rev. Phys. Chem.* **2002**, *53*, 319−348.
(3) Hoffmann, R. A Chemical and Theoretical way to look at Bonding on Surfaces. *Rev. Mod. Phys.* **1988**, *60*, 601.
(4) Hammer, B.; Nørskov, J. K. Electronic Factors Determining the Reactivity of Metal Surfaces. *Surf. Sci.* **1995**, *343*, 211−220.
(5) Hammer, B.; Nielsen, O. H.; Nørskov, J. K. Structure Sensitivity in Adsorption: CO Interaction with Stepped and Reconstructed Pt Surfaces. *Catal. Lett.* **1997**, *46*, 31−35.
(6) Wan, K. T.; Davis, M. E. Design and Synthesis of a Heterogeneous Asymmetric Catalyst. *Nature* **1994**, *370*, 449−450.
(7) Mondloch, J. E.; Bayram, E.; Finke, R. G. A review of the kinetics and mechanisms of formation of supported-nanoparticle heterogeneous catalysts. *J. Mol. Catal. A: Chem.* **2012**, *355*, 1−38.
(8) Rodriguez, J. A.; Jirsak, T.; Chaturvedi, S.; Hrbek, J. Surface Chemistry of SO_2 on Sn and Sn/Pt(111) Alloys: Effect of Metal-Metal Bonding on Reactivity toward Sulfur. *J. Am. Chem. Soc.* **1998**, *120*, 11149−11157.
(9) Batzill, M.; Beck, D. E.; Koel, B. E. Electronic Contrast in Scanning Tunneling Microscopy of Sn−Pt (111) Surface Alloys. *Surf. Sci.* **2000**, *466*, L821−L826.
(10) Delbecq, F.; Sautet, P. Influence of Sn Additives on the Selectivity of Hydrogenation of α-β-Unsaturated Aldehydes with Pt Catalysts: A Density Functional Study of Molecular Adsorption. *J. Catal.* **2003**, *220*, 115−126.
(11) Blyholder, G. J. Molecular Orbital View of Chemisorbed Carbon Monoxide. *Phys. Chem.* **1964**, *68*, 2772−2777.
(12) Kresse, G.; Furthmüller, J. Efficient Iterative Schemes for ab initio Total-Energy Calculations using a Plane-Wave Basis Set. *Phys. Rev. B* **1996**, *54*, 11169.
(13) (a) Dion, M.; Rydberg, H.; Schröder, E.; Langreth, D. C.; Lundqvist, B. I. Van der Waals Density Functional for General Geometries. *Phys. Rev. Lett.* **2004**, *92*, 246401. (b) Zhang, Y.; Yang, W. Comment on "Generalized Gradient Approximation Made Simple". *Phys. Rev. Lett.* **1998**, *80*, 890.
(14) Lazic, P.; Alaei, M.; Atodiresei, N.; Caciuc, V.; Brako, R.; Blügel, S. Density Functional Theory with Nonlocal Correlation: A Key to the Solution of the CO Adsorption Puzzle. *Phys. Rev. B* **2010**, *81*, No. 045401.
(15) Perdew, J. P.; Burke, K.; Ernzerhof, M. Generalized Gradient Approximation Made Simple. *Phys. Rev. Lett.* **1996**, *77*, 3865.
(16) Dudarev, S. L.; Botton, G. A.; Savrasov, S. Y.; Humphreys, C. J.; Sutton, A. P. Electron-Energy-Loss Spectra and the Structural Stability of Nickel Oxide: An LSDA+ U Study. *Phys. Rev. B* **1998**, *57*, 1505.
(17) Patra, A.; Peng, H.; Sun, J.; Perdew, J. P. Rethinking CO Adsorption on Transition-Metal Surfaces: Effect of Density-Driven Self-Interaction Errors. *Phys. Rev. B* **2019**, *100*, No. 035442.
(18) Medeiros, P. V. C.; Stafström, S.; Björk, J. Effects of Extrinsic and Intrinsic Perturbations on the Electronic Structure of Graphene: Retaining an Effective Primitive Cell Band Structure by Band Unfolding. *Phys. Rev. B* **2014**, *89*, No. 041407.
(19) Medeiros, P. V. C.; Tsirkin, S. S.; Stafström, S.; Björk, J. Unfolding Spinor Wave Functions and Expectation Values of General

Operators: Introducing the Unfolding-Density Operator. *Phys. Rev. B* **2015**, *91*, No. 041116.
(20) Ebert, H.; Ködderitzsch, D.; Minár, J. Calculating Condensed Matter Properties Using the KKR-Green's Function Method—Recent Developments and Applications. *Rep. Prog. Phys.* **2011**, *74*, No. 096501.
(21) Kalhara Gunasooriya, G. T. K.; Saeys, M. CO Adsorption Site Preference on Platinum: Charge is the Essence. *ACS Catal.* **2018**, *8*, 3770−3774.
(22) Luttinger, J. M.; Ward, J. C. Ground-State Energy of a Many-Fermion System. II. *Phys. Rev.* **1960**, *118*, 1417−1427.
(23) Luttinger, J. M. Fermi Surface and Some Simple Equilibrium Properties of a System of Interacting Fermions. *Phys. Rev.* **1960**, *119*, 1153−1163.
(24) Paffet, M. T.; Gebhard, S. C.; Windham, R. G.; Koel, B. E. Chemisorption of Carbon Monoxide, Hydrogen, and Oxygen on Ordered Tin/Platinum (111) Surface Alloys. *J. Phys. Chem.* **1990**, *94*, 6831−6839.
(25) Dupont, C.; Loffreda, D.; Delbecq, F.; Jugnet, Y. Vibrational Study of CO Chemisorption on the Pt3Sn (111)-(2× 2) Surface. *J. Phys. Chem. C* **2007**, *111*, 8524−8531.
(26) Kresse, G.; Gil, A.; Sautet, P. Significance of Single-Electron Energies for the Description of CO on Pt (111). *Phys. Rev. B* **2003**, *68*, No. 073401.
(27) Chou, K. C.; Westerberg, S.; Shen, Y. R.; Ross, P. N.; Somorjai, G. A. Probing the Charge-Transfer State of CO on Pt (111) by Two-Dimensional Infrared-Visible Sum Frequency Generation Spectroscopy. *Phys. Rev. B* **2004**, *69*, 153413.
(28) Nakatsuji, H.; Morita, H.; Nakai, H.; Murata, Y.; Fukutani, K. Theoretical Study on the Photostimulated Desorption of CO from a Pt Surface. *J. Chem. Phys.* **1996**, *104*, 714−726.

https://doi.org/10.1021/acscatal.1c04566
ACS Catal. 2022, 12, 219−225